RSC Advances

PAPER

View Article Online
View Journal | View Issue

Cite this: *RSC Adv.*, 2020, **10**, 37989

Thiolated poly(aspartic acid)-functionalized two-dimensional MoS_2, chitosan and bismuth film as a sensor platform for cadmium ion detection†

Qiang Cao,‡[ab] Yushi Xiao,‡[ab] Rong Huang,‡[ac] Na Liu,[ab] Hai Chi,[d] Cheng-Te Lin,[e] Chi-Hsien Huang,[f] Gang Han[a] and Lidong Wu *[a]

Received 16th July 2020
Accepted 6th October 2020

DOI: 10.1039/d0ra06197b

rsc.li/rsc-advances

In this work, a sensitive electrochemical platform for determination of cadmium ions (Cd^{2+}) is obtained using thiolated poly(aspartic acid) (TPA)-functionalized MoS_2 as a sensor platform by differential pulse anodic stripping voltammetry (DPASV). The performance of the TPA–MoS_2-modified sensor is systemically studied. It demonstrates that the TPA–MoS_2 nanocomposite modified sensor exhibits superior analytical performance for Cd^{2+} over a linear range from 0.5 μg L^{-1} to 50 μg L^{-1}, with a detection limit of 0.17 μg L^{-1}. Chitosan is able to form a continuous coating film on the surface of the GC electrode. The good sensing performance of the TPA–MoS_2-modified sensor may be attributed to the following factors: the large surface area of MoS_2 (603 m^2 g^{-1}), and the abundant thiol groups of TPA. Thus, the TPA–MoS_2-modified sensor proves to be a reliable and environmentally friendly tool for the effective monitoring of Cd^{2+} existing in aquacultural environments.

1. Introduction

Cadmium (Cd) is one of the priority pollutants due to its high toxicity.[1–3] Cd^{2+} not only causes renal tubular dysfunction and bone degeneration (itai-itai disease),[4–6] but is also classified as a carcinogenic chemical by the International Agency for Research on Cancer (IARC).[7–9] Traditionally, inductively coupled plasma mass spectrometry (ICP-MS),[10,11] atomic absorption spectrometry (ABS)[12–14] and ion chromatography[15,16] are used for detecting Cd^{2+}. Although these instruments have good precision and high resolution, they are too expensive and labor-intensive.[17,18] Therefore, it is urgent to develop a sensitive method to protect our food, medicine and drinking water from Cd^{2+} pollution.

The electrochemical sensor is one of the most promising tools for detecting Cd^{2+} due to its low cost, rapid speed, portability and reliability.[19–21] Mercury modified electrode has been intensively used for detecting trace Cd^{2+} by differential pulse anodic stripping voltammetry (DPASV).[22,23] However, the toxicity of mercury severely limits its applications in constructing sensors.[24,25] Therefore, bismuth, the less toxicity heavy metal,[26,27] is used for constructing sensors in this work. Except electrode materials, the sensing material also plays an important role in constructing sensors.[28]

As is well known, 2D materials have been established for the sensitive detection methods of environmental pollutants.[29–32] Molybdenum disulfide (MoS_2) is one of transition-metal dichalcogenides (TMDs), which has a typical layered structure formed by a stack of planes.[33–35] Each layer of MoS_2 consists of three atom layers (S–Mo–S), a layer of molybdenum atoms sandwiched between two layers of sulfur atoms.[36–38] These triple layers are weakly held together by van der Waals forces.[39–41] MoS_2 has unique properties including good flexibility, a tunable bandgap energy controlled by the number of layers and planar electric transportation property.[42–45] Due to its fascinating characteristics, MoS_2 has received much attention for construction of promising electronics devices, for example, field-effect transistors, lithium-ion batteries, *etc.*[46–49] However, exploring more binding sites on MoS_2 for Cd^{2+} is still challenging, and this is the key to achieve excellent low detection limit and sensitivity. The poor surface modification of MoS_2 limits its application as electrode material for constructing electrochemical sensors.[50]

[a]*Key Laboratory of Control of Quality and Safety for Aquatic Products, Chinese Academy of Fishery Sciences, Beijing, 100141, China. E-mail: wulidong19849510@hotmail.com; Fax: +86-10-68690712; Tel: +86-10-68690712*

[b]*Shanghai Ocean University, Shanghai 201306, China*

[c]*Beijing Engineering and Technology Research Center of Food Additives, Beijing Technology and Business University (BTBU), Beijing, 100048, China*

[d]*East China Sea Fisheries Research Institute, Chinese Academy of Fishery Sciences, Shanghai, 201306, China*

[e]*Ningbo Institute of Materials Technology and Engineering, Chinese Academy of Sciences, Ningbo, 315201, China*

[f]*Department of Materials Engineering, Mingchi University of Technology, 243303, Taiwan*

† Electronic supplementary information (ESI) available. See DOI: 10.1039/d0ra06197b

‡ Authors equally contribution to this work.

To address this critical challenge, it is predicted that controllable surface modification of MoS_2 could significantly improve the sensitivity of MoS_2 based sensor.[51,52] Thus, in this work, thiolated polymers are chemically adsorbed on electron-rich MoS_2 through covalent bonding. The sulfur on the MoS_2 surface plays as a soft Lewis base showing a high affinity for heavy metal ions (*e.g.*, Bi^{3+}, Cd^{2+}). MoS_2 demonstrates both a high adsorption capacity due to abundant sulfur adsorption sites and fast kinetics due to easy access to these sites. Therefore, thiolated polymer modified MoS_2 plays as one of the most effective platforms for detecting Cd^{2+}. It shows that this sensor possesses superior stability, sensitivity and LOD. The proposed sensor can be used as an environmental-friendly "pre-alarm" tool for rapid determining Cd^{2+} in aquaculture water, Chinese drug, food and beverage.

2. Experimental section

2.1. Materials and solutions

Cadmium chloride, bismuth chloride, and other chemicals are from Tianjin Kermel (Tianjin, China). Thiolated poly(aspartic acid) is obtained from Covestro company (Shanghai, China). 100 mmol L^{-1} pH 6.5 acetate buffer is used as the electrolyte in electrochemical experiments.

2.2. Apparatus

A JEM-2100 instrument (Japan) is used for obtaining transmission electron microscopy (TEM) images. Scan electron microscopy (SEM) images are obtained by Zeiss Sigma 300 (Germany). A CHI 660B Electrochemical Workstation (Shanghai, China) is used for testing Cd^{2+} through DPASV. A functionalized MoS_2 and chitosan film modified glassy carbon (GC) electrode is the working electrode, the Ag/AgCl electrode is the reference electrode, and the platinum wire is the auxiliary electrode. The concentration of Cd^{2+} is also confirmed through atomic absorption spectrometry (AAS, Jena, Germany).

2.3. Preparation of MoS_2 and modification of GC electrode

MoS_2 nanosheets are prepared by an ultrasonic exfoliation method as literature reported.[53] 1.0 g MoS_2 powder is added into 10 mL *N*-methyl-pyrrolidone solution under ultrasonic wave for 2 h at 0 °C. After centrifugation at 7000 rpm for 30 min, the prepared MoS_2 nanosheets is dispersed in the supernatant. The 1 mL of 1 mg mL^{-1} prepared MoS_2 is mixed with 1 mL 2 mg mL^{-1} thiolated poly(aspartic acid) (TPA), and vibrated by vortex for 12 h at room temperature.

The GC electrode is polished by alumina powder (0.05 μm) and washed by ethanol for three times, respectively. Then, 5 μL 0.6 mg mL^{-1} functionalized MoS_2 solution, 5 μL chitosan (8 wt%) and 10 μL Milli-Q water are mixed. Finally, 5 μL mixture is immobilized onto the GC electrode to obtain a TPA–MoS_2/GC electrode.

2.4. Cd^{2+} detection by TPA–MoS_2/GC electrode

Bismuth film is plated on the TPA–MoS_2/GC electrode through the electrodeposition of 10 mg L^{-1} Bi^{3+} for 210 s with stirring. After coating bismuth film, Cd^{2+} is monitored by the TPA–MoS_2/GC electrode in 8 mL 100 mmol L^{-1} acetate buffer (pH 6.5).

3. Results and discussion

3.1. TEM characterization of MoS_2

MoS_2 was obtained through ultrasonic exfoliation method. Fig. 1 showed representative TEM images of the MoS_2 nanosheets (A), the functionalized MoS_2 (B) and the functionalized MoS_2 deposited with bismuth and cadmium (C). It suggested that the prepared MoS_2 nanosheets were very thin and clear. After TPA non-covalent modified on the MoS_2 nanosheets, the original morphology of the MoS_2 nanosheets was retained in the composites. Fig. 1C is a TEM image of the TPA–MoS_2–Bi–Cd nanocomposites and clearly showed the modification of the MoS_2 by Bi and Cd nanocluster. As shown in Fig. S1,† TPA–MoS_2 surface becomes rough and there are lots of nanoparticles on the surface of TPA–MoS_2 after detection. It is consistent with TEM images. FTIR was also used to confirm the formation of TPA on the MoS_2 nanosheets. As shown in Fig. 2, the peak of 2550 cm^{-1} was the SH group of TPA. After TPA modified on the MoS_2 nanosheets, the absorption bands at 1390 (symmetric stretching of –COOH), 1600 (asymmetric stretching of –COOH), and 3000–3500 cm^{-1} (NH_3^+ stretch) became weak. The change in their dipole moment was due to TPA modification on the MoS_2 nanosheets. These results showed the successful modification of TPA on the MoS_2 nanosheets. X-ray photoelectron spectroscopy (XPS) was used to determine the chemical composition and states of the TPA–MoS_2

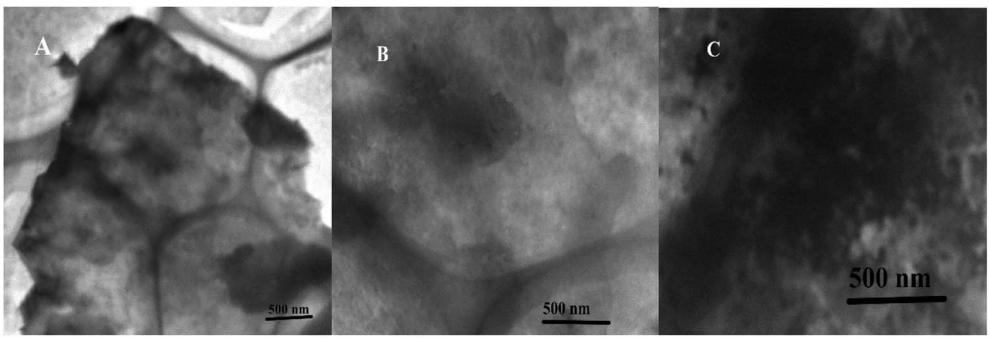

Fig. 1 TEM image of MoS_2 nanosheets (A), the TPA functionalized MoS_2 (B), and the TPA–MoS_2 with bismuth and cadmium (C).

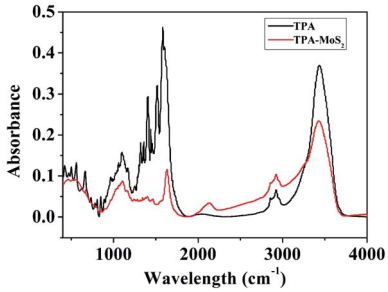

Fig. 2 FTIR image of TPA and TPA–MoS_2.

with cadmium. As shown in Fig. S2A,† two peaks at 229 and 232 eV energy values ascribed to Mo core peaks, and the peak at 226 eV ascribed to S core peak. Fig. S2B† showed two peaks at 163 and 161.7 eV. These binding energy values are consistent with the expected charge states of Cd^{2+}, Mo^{4+} and S^{2-}. Furthermore, the specific surface area of the MoS_2 nanosheets was estimated by the Brunauer–Emmett–Teller (BET) method. Its specific surface area achieved to be 603 m^2 g^{-1}. The high effective surface area and high-quality of MoS_2 could provide good performances for GC electrode.

3.2. Electrochemical characterization of the TPA–MoS_2-modified GC electrode

Cyclic voltammetry (CV) was an electrochemical measurement method which could be used for monitoring the preparation procedure of GC electrode. As shown in Fig. 3, the immobilization process of the TPA–MoS_2/GC electrode was performed. Fig. 3 displayed the CVs of the bare GC, MoS_2/GC and TPA–MoS_2/GC electrodes in 2 mmol L^{-1} $K_3[Fe(CN)_6]/K_4[Fe(CN)_6]$ solution. The CV of the bare GC electrode was highest among these electrodes. It demonstrated that the electron transfer rate between $[Fe(CN)_6]^{3-/4-}$ and the bare electrode was very fast. The CV of the TPA–MoS_2/GC electrode was the lowest, which demonstrated that a chitosan film and TPA–MoS_2 had covered on the surface of the bare GC electrode. Without modification of

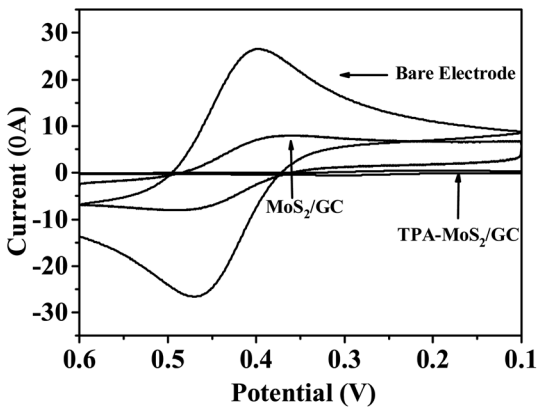

Fig. 3 Cyclic voltammograms of bare GC, MoS_2/GC and TPA–MoS_2/GC electrodes in 2 mmol L^{-1} $[Fe(CN)_6]^{3-/4-}$ at a scan rate of 100 mV s^{-1}.

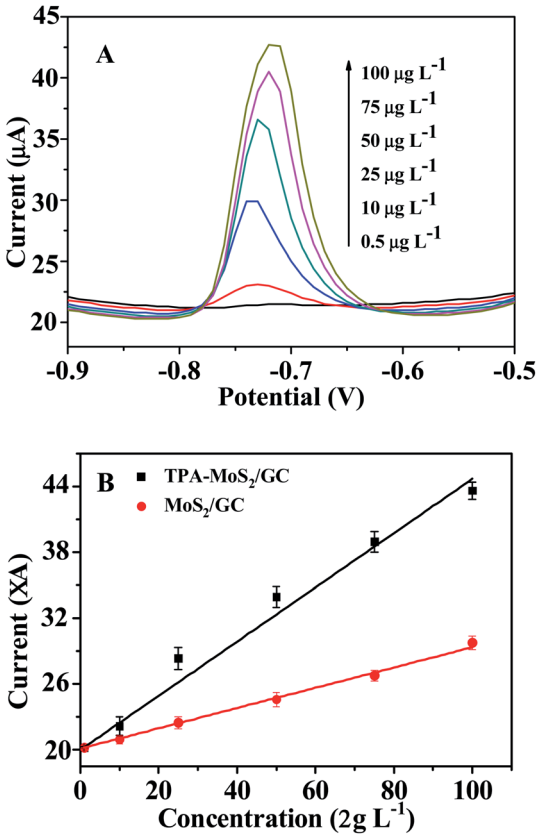

Fig. 4 (A) DPASVs obtained for different concentrations of Cd^{2+} using a bismuth-coated TPA–MoS_2/GC electrode; from bottom to top, 0.5, 10, 25, 50, 75, 100 μg L^{-1} with 10 mg L^{-1} Bi^{3+} electrodeposited for 210 s under stirring in 100 mmol L^{-1} acetate buffer (pH 5.0). (B) Calibration curves of MoS_2/GC (red color) and TPA–MoS_2/GC (black color) electrodes for Cd^{2+}.

TPA, the MoS_2 nanosheets possessed good conductivity, and the CV of the chitosan–MoS_2/GC electrode was higher than the TPA–MoS_2/GC electrode. The results might be due to the introduction of TPA, which played a key role in improving the binding sites of Cd^{2+}. It also showed that the TPA–MoS_2 and chitosan film had covered on the GC electrode.

3.3. The TPA–MoS_2-modified GC electrode for Cd^{2+} analysis

In this study, DPASV was used for detecting Cd^{2+}. Fig. 4A showed that the DPASVs of the MoS_2/GC and the TPA–MoS_2/GC electrodes increased with the concentrations of Cd^{2+} from 0.5 to 100 μg L^{-1} in 100 mmol L^{-1} acetate buffer (pH 6.5) with 10 mg L^{-1} Bi^{3+} electrodepositing for 210 s. After the concentrations of Cd^{2+} achieved 150, 200 and 250 μg L^{-1}, the DPASVs of these electrodes increased unobvious. The DPASVs response signals increased linear from 0.5 to 100 μg L^{-1} then become flat. As shown in Fig. 4B, the current peaks increased linearly with Cd^{2+} concentration, and the correlation coefficients was approximate 0.99. The sensitivity of the MoS_2/GC and the TPA–MoS_2/GC electrodes were 101.8 and 178.2 mA cm^{-2} m^{-1}, respectively. Furthermore, the detection limit (DL) was an

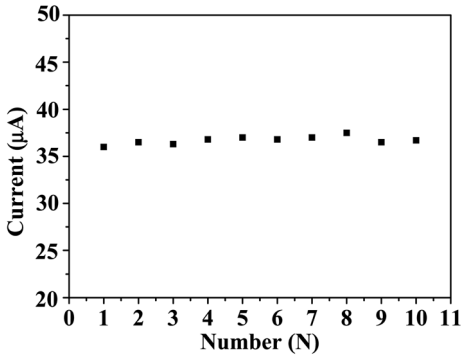

Fig. 5 The stability of 10 repetitive measurements of 50 μg L^{-1} Cd^{2+} in 0.1 mol L^{-1} acetate buffer (pH 5.0) containing 3 mg L^{-1} Bi^{3+}.

Table 1 Comparison of Cd^{2+} concentration in different aquaculture water samples by the sensor and AAS method

Sample	Concentration (μg L^{-1}) (sensor method)	Concentration (μg L^{-1}) (AAS method)	Difference[a] (%)
A	1.9	1.7	11.76
B	—	—	—
C	—	—	—
D	2.1	2.4	−12.5
E	—	—	—
F	—	—	—

[a] Difference = (sensor(value) − AAS(value))/AAS(value) × 100%.

important parameter as sensors. The DL of the TPA–MoS_2/GC and the MoS_2/GC electrodes achieved 0.2 μg L^{-1} and 0.5 μg L^{-1} at a signal-to-noise ratio of 3, respectively. It demonstrated that the DL (0.2 μg L^{-1}) of the TPA–MoS_2/GC electrode was much lower than the standard for detecting tap water quality in China (GB 5749-2006, Cd 0.005 mg L^{-1}). The DL of the TPA–MoS_2/GC electrode was superior to that of the chitosan-multiwalled carbon nanotubes/GC electrode (0.4 μg L^{-1}, electrodepositing Bi^{3+} for 300 s). Reproducibility was another important parameter of sensors. As shown in Fig. 5, 10 repeated measurements for 50 μg L^{-1} Cd^{2+} had excellent reproducibility with relative standard deviation (RSD) of 0.41%. Therefore, this prepared sensor could be potentially applied to rapid detection of Cd^{2+} in the aquaculture water.

Table 2 Analysis of Cd^{2+} by different reported methods

Electrode	Detection limit (μg L^{-1})	Deposition time (s)	Ref.
TPA–MoS_2	0.17	210	Present work
Bi-coated GC	50	120	54
Bi-GP-CNT/GC	0.6	150	55
Bi-Nafion/GC	1.39	120	56

3.4. The TPA–MoS_2/GC electrode testing aquaculture water samples

This sensor was used for detecting Cd^{2+} in the aquaculture water samples. The test samples were directly added into the bottle without enrichment, and then detected by the TPA–MoS_2/GC electrode according to previous procedure. The Cd^{2+} standard solution (50 μg L^{-1}) was added into the bottle to calculate and correct the results of the test samples. A 0.22 μm filter membrane was used for extracting 6 aquaculture water samples. As shown in Table 1, the Cd^{2+} concentration in aquaculture water A and aquaculture water D were 1.9 and 2.1 μg L^{-1}, respectively. For other samples (sample B, sample C, sample E and sample F), there was no Cd^{2+}. The concentration of aquaculture water samples was validated by AAS. It indicated that the sensor was a reliable and sensitive tool for the rapid detection of Cd^{2+} in real samples.

The good sensing performance of the TPA–MoS_2/GC electrode might be attributed to the following factors: the large surface area of MoS_2 greatly increased the active surface area of the GC electrode for Cd^{2+} adsorption, and the abundant thiol group of TPA significantly increased the binding sites for Cd^{2+} (Scheme 1); the good electric conductivity of MoS_2 could improve the electron transfer rate between the surface of the GC electrode and Cd^{2+} in the bulk solution; and the 2D nanostructure provided a very broad space for the easy transfer of Cd^{2+}. Based on these reasons, the TPA–MoS_2/GC electrode exhibited low DL and good reproducibility (Table 2). Thus, the TPA–MoS_2/GC electrode showed greater potential for use as a "pre-alarm" tool.

4. Conclusion

In summary, the TPA–MoS_2/GC electrode was prepared for Cd^{2+} detection in the aquaculture water samples. It showed that the TPA–MoS_2 nanocomposites offered significant advantages, such as low DL and good reproducibility. The good results were

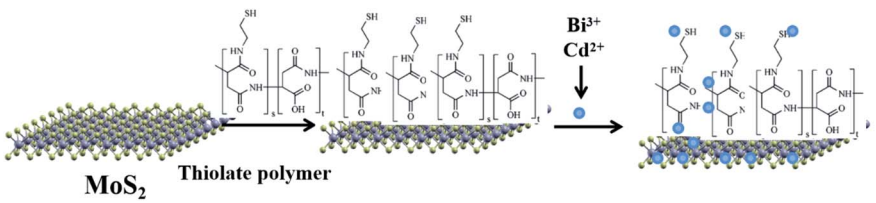

Scheme 1 Schematic diagram of Cd^{2+} absorption on TPA–MoS_2 nanocomposites.

attributed to the large specific surface area, abundant thiol group from TPA and high electrical conductivity of the TPA–MoS_2 nanocomposites. Furthermore, the bismuth electrode provided more environmental-friendly electrode for researcher health. The TPA–MoS_2/GC electrode possessed greatly potential for its application in the on-site rapid analysis of Cd^{2+} in the water or food.

Conflicts of interest

There is no conflicts of interest.

Acknowledgements

This work was supported by the Central Public-interest Scientific Institution Basal Research Fund, CAFS (No. 2020GH09 and 2020TD75).

References

1 Q. Zhao, H. Wang, Y. Du, H. J. Rogers, Z. Wu, S. Jia, X. Yao, F. Xie and W. Liu, *J. Agric. Food Chem.*, 2020, **68**, 1974–1985.
2 C. O. Ogunkunle, D. A. Odulaja, F. O. Akande, M. Varun, V. Vishwakarma and P. O. Fatoba, *J. Biotechnol.*, 2020, **310**, 54–61.
3 Y. S. Kim, M. Y. Song, J. S. Kim, D. S. Rha, Y. J. Jeon, J. E. Kim, H. Y. Ryu, I. J. Yu and K. S. Song, *Toxicol. Res.*, 2009, **25**, 140–146.
4 A. Al-Ghafari, E. Elmorsy, E. Fikry, M. Alrowaili and W. G. Carter, *PLoS One*, 2019, **14**, e0225341.
5 L. Knani, M. Venditti, S. Kechiche, M. Banni, I. Messaoudi and S. Minucci, *Toxicol. Mech. Methods*, 2019, 1–9.
6 X. Li, R. Li, J. Yan, Y. Song, J. Huo, Z. Lan, J. Chen and L. Zhang, *J. Appl. Toxicol.*, 2020, **40**, 352–362.
7 P. Chen, X. Duan, M. Li, C. Huang, J. Li, R. Chu, H. Ying, H. Song, X. Jia, Q. Ba and H. Wang, *Toxicol. Appl. Pharmacol.*, 2016, **310**, 150–158.
8 *IARC Monogr. Eval. Carcinog. Risk Chem. Man*, 1976, **11**, 1–293.
9 N. Degraeve, *Mutat. Res.*, 1981, **86**, 115–135.
10 B. Yan, M. P. Isaure, S. Mounicou, H. Castillo-Michel, W. De Nolf, C. Nguyen and J. Y. Cornu, *Environ. Pollut.*, 2020, **260**, 113987.
11 N. Zhang, K. Shen, X. Yang, Z. Li, T. Zhou, Y. Zhang, Q. Sheng and J. Zheng, *Food Chem.*, 2018, **264**, 462–470.
12 N. A. Kasa, E. Akkaya, B. T. Zaman, G. Cetin and S. Bakirdere, *Environ. Monit. Assess.*, 2018, **190**, 589.
13 M. Shirani, S. Habibollahi and A. Akbari, *Food Chem.*, 2019, **281**, 304–311.
14 O. Zverina, J. Kuta, P. Coufalik, P. Koseckova and J. Komarek, *Food Chem.*, 2019, **298**, 125084.
15 B. Paull, E. Twohill and W. Bashir, *J. Chromatogr. A*, 2000, **877**, 123–132.
16 S. Tanikkul, J. Jakmunee, S. Lapanantnoppakhun, M. Rayanakorn, P. Sooksamiti, R. E. Synovec, G. D. Christian and K. Grudpan, *Talanta*, 2004, **64**, 1241–1246.
17 M. Xu, R. Ma, C. Huang, G. Shi, T. Zhou and J. Deng, *Anal. Chim. Acta*, 2020, **1096**, 174–183.
18 M. Zhou, Y. Wu, J. Zhang, Y. Zhang, X. Chen, J. Ye and S. Wang, *Anal. Sci.*, 2019, **35**, 283–287.
19 K. M. Hassan, G. M. Elhaddad and M. AbdelAzzem, *Mikrochim. Acta*, 2019, **186**, 440.
20 Y. Chen, D. Zhang, D. Wang, L. Lu, X. Wang and G. Guo, *Talanta*, 2019, **202**, 27–33.
21 L. Wu, X. Fu, H. Liu, J. Li and Y. Song, *Anal. Chim. Acta*, 2014, **851**, 43–48.
22 M. F. De Oliveira, A. A. Saczk, L. L. Okumura, A. P. Fernandes, M. De Moraes and N. R. Stradiotto, *Anal. Bioanal. Chem.*, 2004, **380**, 135–140.
23 E. Nagles, V. Arancibia, C. Rojas and R. Segura, *Talanta*, 2012, **99**, 119–124.
24 Z. J. Suturovic, S. Z. Kravic, Z. S. Stojanovic, A. D. Durovic and T. Z. Brezo-Borjan, *J. Anal. Methods Chem.*, 2019, **2019**, 3579176.
25 M. Mladenov, V. Mirceski, I. Gjorgoski and B. Jordanoski, *Bioelectrochemistry*, 2004, **65**, 69–76.
26 N. B. Li, W. W. Zhu, J. H. Luo and H. Q. Luo, *Analyst*, 2012, **137**, 614–617.
27 H. Li, J. Li, Z. Yang, Q. Xu, C. Hou, J. Peng and X. Hu, *J. Hazard. Mater.*, 2011, **191**, 26–31.
28 S. Cerovac, V. Guzsvany, Z. Konya, A. M. Ashrafi, I. Svancara, S. Roncevic, A. Kukovecz, B. Dalmacija and K. Vytras, *Talanta*, 2015, **134**, 640–649.
29 J. Tu, Y. Gan, T. Liang, Q. Hu, Q. Wang, T. Ren, Q. Sun, H. Wan and P. Wang, *Front. Chem.*, 2018, **6**, 333.
30 Q. Wang, Z. Zhou, Y. Zhai, L. Zhang, W. Hong, Z. Zhang and S. Dong, *Talanta*, 2015, **141**, 247–252.
31 J. Liu, L. Han, T. Wang, W. Hong, Y. Liu and E. Wang, *Chem.–Asian J.*, 2012, **7**, 2824–2829.
32 J. M. Lim, D. Kim, Y. G. Lim, M. S. Park, Y. J. Kim, M. Cho and K. Cho, *J. Mater. Chem. A*, 2015, **3**, 7066–7076.
33 L. O. Jones, M. A. Mosquera, M. A. Ratner and G. C. Schatz, *ACS Appl. Mater. Interfaces*, 2020, **12**, 4607–4615.
34 Z. Han, Z. Tang, K. Jiang, Q. Huang, J. Meng, D. Nie and Z. Zhao, *Biosens. Bioelectron.*, 2020, **150**, 111894.
35 Z. Chen, C. Liu, J. Liu, J. Li, S. Xi, X. Chi, H. Xu, I. H. Park, X. Peng, X. Li, W. Yu, X. Liu, L. Zhong, K. Leng, W. Huang, M. J. Koh and K. P. Loh, *Adv. Mater.*, 2020, **32**, e1906437.
36 F. I. Alzakia, W. Sun, S. J. Pennycook and S. C. Tan, *ACS Appl. Mater. Interfaces*, 2020, **12**, 3096–3103.
37 W. Lu, P. Yu, M. Jian, H. Wang, H. Wang, X. Liang and Y. Zhang, *ACS Appl. Mater. Interfaces*, 2020, **12**, 16822.
38 C. L. C. Rodriguez, P. A. R. Munoz, K. Z. Donato, L. Seixas, R. K. Donato and G. J. M. Fechine, *Phys. Chem. Chem. Phys.*, 2020, **22**, 1457–1465.
39 E. M. Alexeev, D. A. Ruiz-Tijerina, M. Danovich, M. J. Hamer, D. J. Terry, P. K. Nayak, S. Ahn, S. Pak, J. Lee, J. I. Sohn, M. R. Molas, M. Koperski, K. Watanabe, T. Taniguchi, K. S. Novoselov, R. V. Gorbachev, H. S. Shin, V. I. Fal'ko and A. I. Tartakovskii, *Nature*, 2019, **567**, 81–86.
40 M. M. Furchi, A. Pospischil, F. Libisch, J. Burgdorfer and T. Mueller, *Nano Lett.*, 2014, **14**, 4785–4791.

41 S. Tsoi, P. Dev, A. L. Friedman, R. Stine, J. T. Robinson, T. L. Reinecke and P. E. Sheehan, *ACS Nano*, 2014, **8**, 12410–12417.
42 R. Zhang, Y. Qin, P. Liu, C. Jia, Y. Tang and H. Wang, *ChemSusChem*, 2020, **13**, 1354–1365.
43 Z. Wang, Q. Tu, S. Zheng, J. J. Urban, S. Li and B. Mi, *Nano Lett.*, 2017, **17**, 7289–7298.
44 Y. Yuan, H. Lv, Q. Xu, H. Liu and Y. Wang, *Nanoscale*, 2019, **11**, 4318–4327.
45 Y. Gao, K. Huang, X. Wu, Z. Hou and Y. Liu, *J. Alloys Compd.*, 2018, **741**, 174–181.
46 A. Dankert, L. Langouche, M. V. Kamalakar and S. P. Dash, *ACS Nano*, 2014, **8**, 476–482.
47 H. Liu, M. Si, S. Najmaei, A. T. Neal, Y. Du, P. M. Ajayan, J. Lou and P. D. Ye, *Nano Lett.*, 2013, **13**, 2640–2646.
48 W. Zhang, Y. Song, S. J. He, L. Shang, R. N. Ma, L. P. Jia and H. S. Wang, *Nanoscale*, 2019, **11**, 20910–20916.
49 P. Bi and W. Hong, *Mater. Chem. Phys.*, 2020, **255**, 123577–123583.
50 D. Ma, J. Yu, W. Yin, X. Zhang, L. Mei, Y. Zu, L. An and Z. Gu, *Chemistry*, 2018, **24**, 15868–15878.
51 Y. Chen, X. Wu and K. Huang, *Sens. Actuators, B*, 2018, **270**, 179–186.
52 H. L. Shuai, X. Wu and K. J. Huang, *J. Mater. Chem. B*, 2017, **5**, 5362–5372.
53 A. Gupta, V. Arunachalam and S. Vasudevan, *J. Phys. Chem. Lett.*, 2016, **7**, 4884–4890.
54 J. Wang, J. Lu, S. B. Hocevar, P. A. Farias and B. Ogorevc, *Anal. Chem.*, 2000, **72**, 3218–3222.
55 X. Xuan and J. Y. Park, *Sens. Actuators, B*, 2018, **255**, 1220–1227.
56 J. Li, J. Zhang, H. Wei and E. Wang, *Analyst*, 2009, **134**, 273–277.